Novel Multilayer Electromagnetic Bandgap Structure with Simultaneously Surface-Wave Suppression in the L, S, C and X-bands

1st Diego Lorente
Microwaves and Radar Institute
German Aerospace Center (DLR)
Wessling, Germany
diego.lorentecatalan@dlr.de

2nd Markus Limbach
Microwaves and Radar Institute
German Aerospace Center (DLR)
Wessling, Germany
markus.limbach@dlr.de

3nd Héctor Esteban
Departamento de Comunicaciones
Universitat Politècnica de València (UPV)
Valencia, Spain
hesteban@dcom.upv.es

4nd Vicente E. Boria Esbert
Departamento de Comunicaciones
Universitat Politècnica de València (UPV)
Valencia, Spain
vboria@dcom.upv.es

***Abstract*—In this work, a multiband Electromagnetic Bandgap (EBG) unit-cell (UC), that provides surface-wave suppression in the L, S, C and X-bands, is presented. The proposed design makes use of a group of 2×2 dual-band slotted mushroom UC-EBG, that are resonant at the C-band (5.2 GHz) and X-band (9.6 GHz), to create a tri-band UC-EBG that achieves an additional bandgap at S-band (3.2 GHz). Consequently, a geometrical arrangement of 2×2 tri-band UC-EBG are short-circuited to a single-band mushroom UC, that is resonant at L-band (1.5 GHz), leading to a multilayer UC-EBG structure with quad-band performance. The presented work is thoroughly validated making use of several simulation approaches, in which the different dual-band, tri-band and quad-band EBG configurations are analyzed. The proposed UC-EBG enables, with a single unit-cell design, and without using reconfigurable elements, the simultaneous suppression of surface waves in the L, S, C, and X frequency bands, becoming particularly suitable for multifrequency applications.**

***Index Terms*—electromagnetic bandgap, unit-cell, surface-wave suppression, stopband, quad-band, multilayer.**

I. Introduction

Metamaterials are usually referred as artificial structures that are not found in nature and exhibit singular properties. In microwave and RF applications they are mostly implemented as metal-dielectric unit-cells, that are periodically arranged by an electrically small distance, in terms of the wavelength, in order to synthesize an homogeneous structure.

Among these metamaterial structures, and due to their unique electromagnetic properties, Electromagnetic Bandgaps (EBGs) have attracted much attention in the antenna field [1]. They behave as a high impedance surface, working as a parallel LC network, in which at the frequency of resonance, no surface wave propagates. This surface wave suppression characteristic, also known as bandgap or stopband, makes EBGs convenient to improve the array element isolation [2], to enhance the antenna performance [3] or to reduce the edge diffraction effects [4]. In addition, EBGs can also exhibit artificial magnetic characteristics, providing in-phase reflection, becoming also suitable for low-profile reflectors [5].

However, due to their resonant nature, EBGs only yield their unique electrical properties at a limited frequency band. For this reason, much focus has been placed to enhance the stopband performance of these structures. Some works have investigated broadband EBGs to improve the surface-wave suppression bandwidth by using stacked structures or fractal approaches [6]. Others have proposed multiband EBG-UC designs that achieve several stopbands by means of reconfigurable structures, that make use of active elements [12] or considering different unit-cell geometries [7]–[11]. To the best of author's knowledge, neither multiband EBG structure has been found in literature that provides simultaneously surface-wave suppression at the L-band (1-2 GHz), S-band (2-4 GHz), C-band (4-8 GHz) and X-band (8-11 GHz), that becomes relevant due to the numerous applications in these frequency ranges, nor broadband EBG-UC whose performance covers the aforementioned frequency bands.

For this reason, a novel EBG structure that achieves five different stopbands, covering the frequency range of 1-11 GHz with a single unit-cell design, is presented in this work. Due to its multiband performance, the proposed EBG-UC becomes suitable to be used in a broad range of different areas such as mobile communications, radar, navigation, medical applications, telemetry, etc.

This article is organized as follows: in section II, a tri-band EBG-UC based on a 2×2 grouping of dual-band slotted mushroom unit-cells is designed and analyzed. Consequently, in section III, a geometrical arrangement of 2x2 tri-band unit-cells are connected to a single-band EBG-UC that is resonant at L-band, leading to a quad-band unit-cell design that provides surface-wave suppression at the L, S, C and X-bands. Finally,

the outcomes of the proposed work is discussed in section IV.

II. Tri-band EBG-UC resonant at S, C, and X-band

A tri-band EBG-UC is built from the grouping of 2×2 dual-band slotted mushroom UCs, as depicted in Figure 1. The EBG structure is implemented on a substrate Rogers RT/Duroid 5880 ($\varepsilon_r = 2.2$, $\tan\delta = 0.0009$) with thickness $h_1 = 1.5$ mm. The UCs are separated by a distance g_s that leads to a periodicity of $p_s = WS + g_s$, being WS the unit-cell width. The geometrical parameters are listed in Table I.

Each slotted mushroom type EBG-UC behaves as a parallel LC network, that is designed to be resonant at C-band, by which a capacitance is created between the metallic square patches and an inductance is generated from the current loop between the patches and the via. An extra inductance is also introduced when cutting the slot, providing an additional surface-wave suppression bandgap at X-band.

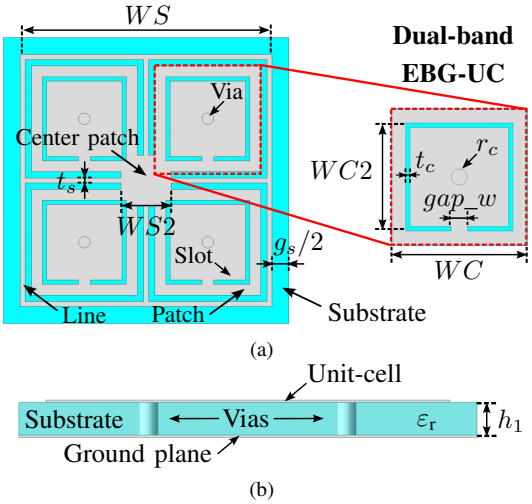

Fig. 1. Tri-band EBG-UC. (a) Top view. (b) Side view.

TABLE I
Geometrical parameters of the tri-band EBG-UC.

WC	6.3 mm	$WC2$	5.0 mm	t_c	0.3 mm
r_c	0.35 mm	gap_w	0.7 mm	g_s	2 mm
WS	15 mm	$WS2$	3 mm	t_s	0.3 mm

Figure 2 shows the dispersion diagram of the dual-band slotted mushroom EBG-UC, calculated in the Brillouin zone and simulated in HFSS with the eigenmode solver and periodic boundaries. Two bandgaps, in which no surface wave propagates, can be clearly identified within the C-band (5.4 GHz∼6.3 GHz) and X-band (9.6 GHz∼10.1 GHz).

To create the tri-band EBG-UC, each of the previous dual-band unit-cells are electrically connected with a centered metallic patch. The resulting increased electrical size provides an additional stopband at a lower frequency range (S-band).

Since the tri-band UC becomes electrically large at higher frequencies, the EBG structure is analyzed considering the waveguide transmission method. The simulated model in HFSS is depicted in Figure 3(a), in which a linear arrangement

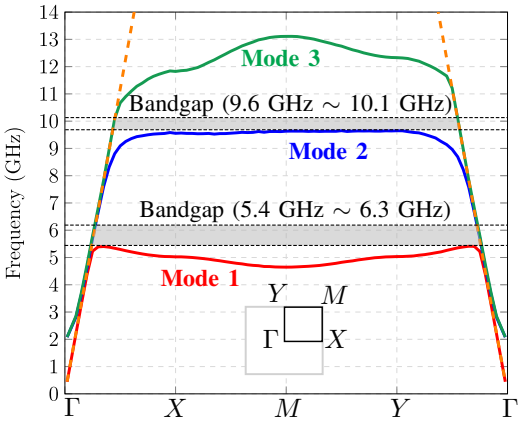

Fig. 2. Simulated dispersion diagram of the dual-band EBG-UC.

of five tri-band unit-cells is inserted in an air box, onto which Perfect Electric Conductor (PEC) boundary conditions on the top and bottom sides, and Perfect Magnetic Conductor (PMC) on the left and right sides, are applied. The simulated S-parameters are plotted in Figure 3(b). The bandgaps can be recognized by those frequency ranges in which full reflection ($|S_{11}| \approx 0$ dB) and no transmission ($|S_{21}| \leq -20$ dB) occurs. Thus, the previous stopbands at the C-band and the X-band, centered approximately at the frequencies of 5.5 GHz and 10 GHz, respectively, can be clearly identified. Furthermore, a new surface-wave suppression band is also achieved at S-band, at the center frequency of 3.2 GHz. It can be also seen an additional bandgap at C-band, centered at 6.9 GHz

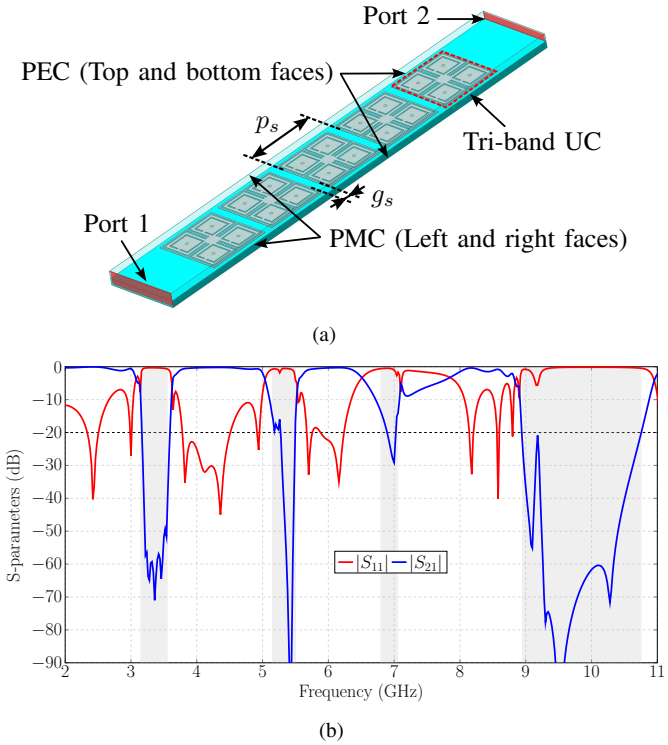

Fig. 3. Simulated tri-band EBG-UC with the waveguide transmission method. (a) HFSS model. (b) S-parameters.

Be noted that in this work, the term tri-band or quad-band refers to the surface-wave suppression in three (S, C and X) and four different frequency bands (L, S, C and X), respectively, and not to the overall number of stopbands.

It can be seen that the stopband performance of the tri-band EBG-UC at the C-band and the X-band slightly differs in comparison with the single slotted mushroom unit-cell, as shown in Figure 2. The reason for that is that the tri-band unit-cell geometry yields additional inductances due to the lines, as well as an extra capacitance between the patches and the lines. Furthermore, the dual-band and tri-band configurations have been analyzed with different simulation methods. While the dispersion diagram of the slotted mushroom is performed analyzing one unit-cell and considering an infinite periodic structure, the waveguide transmission approach considers a finite tri-band EBG structure that it is excited by a TEM mode.

III. Multilayer EBG-UC resonant at L, S, C, and X-band

A quad-band EBG-UC is formed by the arrangement of 2×2 tri-band unit-cells that are short-circuited to a single-band mushroom type EBG of patch width $WL = 35$ mm and via radio $r_L = 1.5$ mm, that is designed to be resonant at L-band. The resulting multilayer unit-cell is depicted in Figure 4.

It can be noted that the single-band unit-cell, that is implemented on a bottom substrate layer of thickness $h_0 = 0.5$ mm, serves as a ground plane for the upper tri-band configuration. Each quad-band unit-cell is separated a distance $g_L = 1$ mm, that has to be small enough to fulfill the periodicity condition at higher frequencies, and to avoid large discontinuities along the ground plane. The values $m_x = m_y = 0.25$ mm assure an uniform spacing in both directions between each tri-band UCs of the same quad-band EBG-UC and among them.

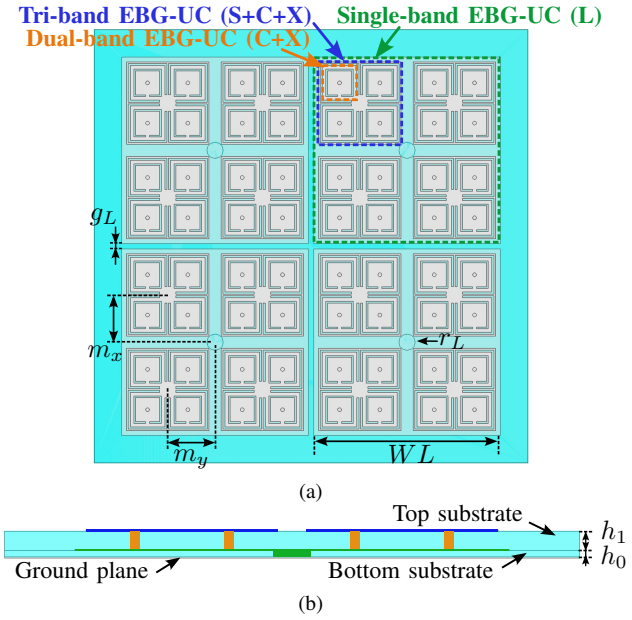

Fig. 4. Multiband EBG-UC. (a) Top view of a geometrical arrangement of 2×2 unit-cells. For depicting purposes the top substrate is transparent. (b) Side view of a single multiband unit-cell.

To characterize the quad-band EBG structure, a waveguide transmission model with five unit-cells is analyzed first. The simulated S-parameters are plotted in Figure 5. It can be seen that the stopband performance is comparable with the tri-band EBG-UC with an additional surface-wave suppression at L-band, centered at 1.5 GHz, thus providing five separated bandgaps along the frequency range of 1-11 GHz. Be noted that due to the broadband characteristics of the quad-band unit-cell and the computational complexity of the simulated model, the analysis is performed running several frequency sweeps. This explains the slight discontinuities at the S-parameters coming from the sensitivity of the logarithmic scala.

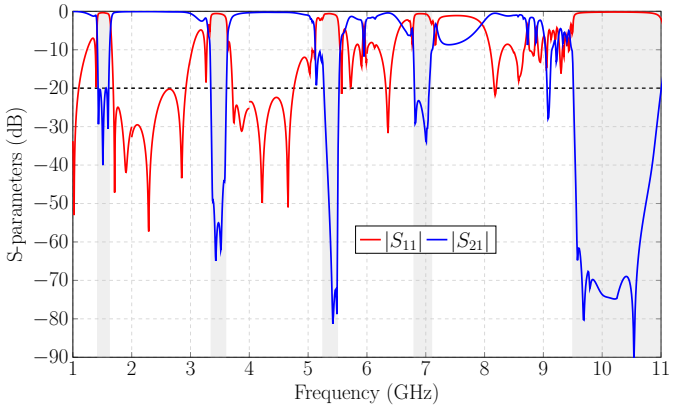

Fig. 5. Simulated S-parameters of the quad-band EBG-UC with the waveguide transmission method considering a linear arrangement of five unit-cells.

To further investigate the proposed quad-band EBG-UC, the structure is analyzed considering a geometrical arrangement of 2×3 unit-cells, that are excited with a suspended microstrip line, as depicted in Figure 6. The feeding line width is 5 mm, and it is placed above the EBG structure, closely located at a distance of 0.5 mm. The overall excitation geometry yields a feeding line impedance of approximately 50 Ω, by which the line separation becomes a trade-off, so the EBG structure can be properly excited by the Quasi-TEM mode of the microstrip line, but without placing it so close that it could affect its performance. In addition, and due to the electrical size of the quad-band EBG-UC and the line width, the position of the feeding line is shifted to properly excite the tri-band UCs.

The simulated results of the suspended transmission line model are plotted in Figure 6. Be noted that the position of the feeding line, placed above the EBG structure, inserts an additional capacitance that can influence the EBG structure by slightly shifting the bandgaps. In addition, this excitation can also lead to some irregularities in the S-parameters, that become more visible due to the broadband frequency range. Nevertheless, it can be seen that the proposed EBG-UC provides, not only surface wave suppression in the L, S, C and X-bands, but also achieves five different stopbands along the frequency range of 1-11 GHz. In addition, and due to the multilayer structure, the bandgap characteristics at L-band can be tuned by modifying the lower single-band unit-cell geometry, as well as the dielectric properties and thickness

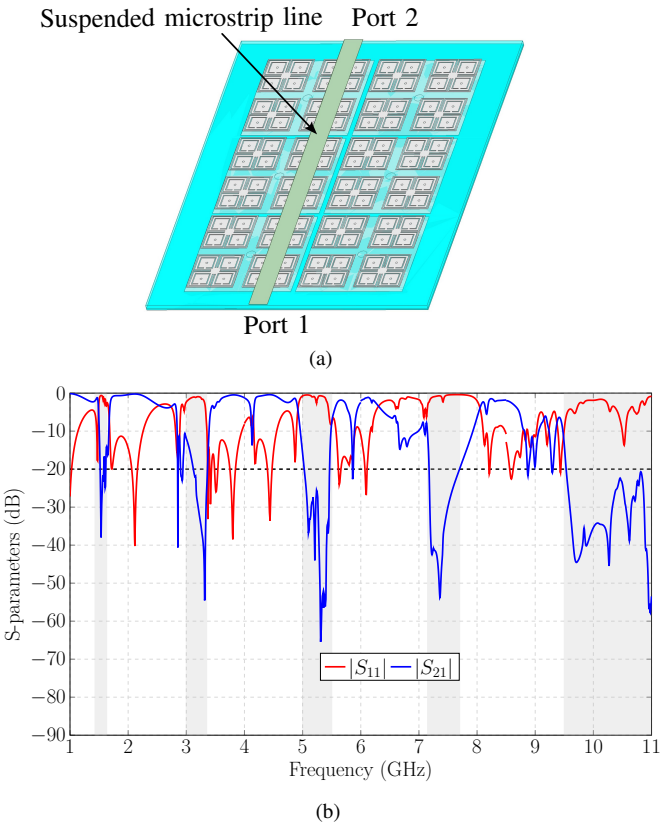

Fig. 6. Simulated quad-band 2×3 EBG structure with the suspended transmission line method. (a) HFSS model. (b) S-parameters.

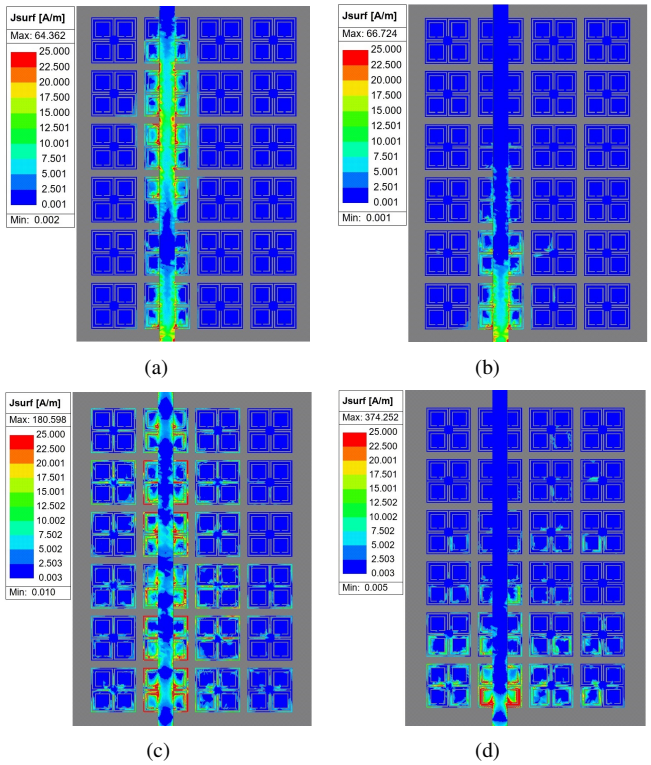

Fig. 7. Magnitude of the induced surface currents on the quad-band EBG structure. (a) Passband at 1.2 GHz (L-band). (b) Stopband at 1.55 GHz (L-band). (c) Passband at 8.6 GHz (X-band). (d) Stopband at 9.7 GHz (X-band).

of the bottom substrate. The same applies for the bandgaps at S, C and X-band regarding the top layer of 2×2 tri-band UCs.

The induced surface currents on the EBG structure, analyzed at the limits of the operational frequency range, namely L-band and X-band, are depicted in Figure 7. It can be noted that, at frequencies where no surface wave propagates (1.55 GHz and 9.7 GHz) no transmission occurs, while outside the bandgaps (1.2 GHz and 8.6 GHz) propagation exists.

IV. Conclusions

In this work, a novel multilayer quad-band EBG-UC structure that provides up to five different stopbands, distributed along the L, S, C and X-band, has been presented. The proposed solution has been analyzed considering several geometrical configurations, based on unit-cell groupings, and validated by means of different simulation methods.

To the best of author's knowledge, the proposed quad-band EBG-UC becomes, not only the first design that achieves simultaneously the surface-wave suppression in the L, S, C and X-bands, but also that provides overall five different stopbands.

References

[1] D. Sievenpiper, Lijun Zhang, R. F. J. Broas, N. G. Alexopolous, and E. Yablonovitch, "High-impedance electromagnetic surfaces with a forbidden frequency band," IEEE Transactions on Microwave Theory and Techniques, vol. 47, pp. 2059-2074 no. 11, Nov. 1999.

[2] S. Dey, S. Dey and S. K. Koul, "Isolation improvement of MIMO antenna using novel EBG, and Hair-Pin shaped DGS at 5G millimeter wave band," IEEE Access, vol. 9, pp. 162820-162834, 2021.

[3] Y. Li, K. Zhang, L. Yang, and L. Du, "Gain enhancement and wideband RCS reduction of a microstrip antenna using triple-band planar electromagnetic band-gap structure," Progress In Electromagnetics Research Letters, Vol. 65, 103-108, 2017.

[4] D. Lorente, M. Limbach, B. Gabler, H. Esteban and V. E. Boria Esbert, "Mitigation of the antenna carrier impact in dual-polarized phased arrays with electromagnetic bandgaps for airborne SAR sensors," 2025 19th European Conference on Antennas and Propagation (EuCAP), Stockholm, Sweden, 2025, pp. 01-05.

[5] S.-H. Kim, T. T. Nguyen, and J.-H. Jang, "Reflection characteristics of 1-d EBG ground plane and its application to a planar dipole antenna," Progress In Electromagnetics Research, Vol. 120, 51-66, 2011.

[6] H. N. B. Phuong, D. N. Chien, and T. M. Tuan, "Novel design of electromagnetic bandgap using fractal geometry," International Journal of Antennas and Propagation, 2013.

[7] N. Kushwaha, and R. Kumar, "Study of different shape electromagnetic band gap (EBG) structures for single and dual band applications," Journal of Microwaves, Optoelectronics and Electromagnetic Applications, vol.13, 2014.

[8] D. Zhang, T. Jiang, and Y. Kong, "A novel compact EBG structure for multi-band wireless communication," 10th International Conference on Wireless Communications, Networking and Mobile Computing (WiCOM 2014), Beijing, 2014, pp. 294-297.

[9] D.-L. Li, M.-S. Zhang, and Z.-X. Wang, "A novel and compact centrosymmetric EBG structure for multiband power noise suppression," IEEE Transactions on Components, Packaging and Manufacturing Technology, vol. 14, no. 9, pp. 1649-1660, Sept. 2024

[10] M.K. Abdulhameed et al., "Novel design of triple-bands EBG," Telkomnika, vol.17, 2019.

[11] P. Jirasakulporn, P. Chomtong, K. Bandudej, and P Akkaraekthalin, Prayoot, "A Compact Triple Band EBG Using Interdigital Coplanar Waveguide Structure for Antenna Gain Enhancement," International Journal of Antennas and Propagation, 2020

[12] R. Dewan, M. K. Rahim, M. Himdi, M. R. Hamid, H. A. Majid, and M. Jalil, "Multiband frequency-reconfigurable antenna using metamaterial structure of electromagnetic band gap," Appl. Phys. A, 2017.